THE JOURNAL OF PHYSICAL CHEMISTRY C

Article

pubs.acs.org/JPCC

Reversible Healing Effect of Water Molecules on Fully Crystallized Metal–Halide Perovskite Film

Wenke Zhou, Yicheng Zhao, Chenglong Shi, Haonan Huang, Jing Wei, Rui Fu, Kaihui Liu, Dapeng Yu, and Qing Zhao*

State Key Laboratory for Mesoscopic Physics and Electron Microscopy Laboratory, School of Physics, Peking University, Beijing 100871, People's Republic of China

Supporting Information

ABSTRACT: Water molecules have been reported to cause the degradation of perovskite crystals by forming a hydrated intermediate structure and then lead iodide irreversibly. Here, the quality of fully crystallized perovskite films is found to be improved by spraying water vapor with an appropriate time. Moreover, this healing effect was found to be reversible and would disappear when the water molecules escaped. Through measuring the steady-state and time-resolved photoluminescence of perovskite film before and after water vapor spray, we found that water molecules can deactivate the nonradiative recombination centers due to hydrogen bonding with uncoordinated ions on the surface of perovskite film. Furthermore, by analyzing the capacitance of devices without and with water vapor spray, the healing or deactivation effect was clearly seen in the significantly decreased density of defect states. This work emphasized the effectiveness of hydroxyl to heal the defects due to dangling bonds on the material surface, and close attention should be paid on searching for more stable healing agent with hydroxyl to increase the efficiency of perovskite solar cells.

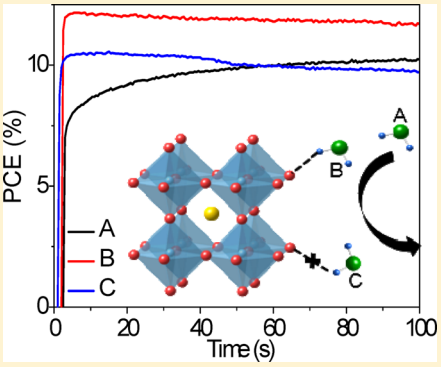

Metal–halide perovskite solar cells have attracted intensive research attention in the past few years due to their solution-based process, low cost, and high power conversion efficiency.[1−13] A high-quality perovskite thin film, containing the properties of high coverage, large grain size, consistent crystal orientation, and low defect concentration, is crucial for a solar cell.[14−17] It has been reported that moisture can lead to the film's degradation and eventually the formation of PbI_2 due to the loss of CH_3NH_3I (MAI), which becomes a serious problem toward commercial-standard stability. Therefore, perovskite films were usually prepared in inert atmosphere (nitrogen, etc.) to resist water molecules. On the other hand, moisture-assisted grain growth or using water as an additive in perovskite precursor has been reported by some groups, and higher quality perovskite films that may be correlated with the reconstruction or recrystallization process during film formation were obtained.[14,18,19] Note that these approaches were applied for the crystallization formation process of perovskite films, which are different from post-treatment to the fully crystallized films discussed further below.

The fully crystallized perovskite films are generally kept in an inert atmosphere to avoid the hydrolysis by water molecules in ambient air, whereas Snaith et al. reported that the fully crystallized perovskite films can be improved by a postmoisture treatment, testified by device performance and steady and time-resolved photoluminescence (PL) tests.[18] The phenomenon was attributed to the fact that water molecules suppress the nonradiative recombination irreversibly by removing excess MAI in perovskite crystals. Nevertheless, the mechanism of how water molecules affect the perovskite film and its related photovoltaic performance remains largely unexplored.

In this article, we demonstrate that the quality of perovskite films and the device performance can be well improved by spraying water vapor onto the as-prepared film. Moreover, this healing effect is found to be reversible if water molecules are removed from perovskite film. A comprehensive investigation on the phase of the perovskite crystal, charge carrier lifetime, recombination time constant, and density of defect states was conducted in order to have a deep understanding on the effect of water molecules on perovskite film. These results indicate that water molecules can heal the defect states in perovskite films. Further, we explore the mechanism behind this healing effect and conclude that a deactivation process of deep-level defects may be the main reason, which originates from the hydrogen bonding between hydroxyl groups in water molecules and iodide ions in perovskite crystals. This study opens up opportunities for further research of molecular modification with hydroxyl on perovskite films to achieve higher quality film and better device photovoltaic performance.

The $CH_3NH_3PbI_3$ ($MAPbI_3$) perovskite films were prepared in a nitrogen-filled atmosphere. The as-made film without any post-treatment is noted as "control sample" (Figure 1a). The

Received: November 24, 2015
Revised: February 16, 2016
Published: February 17, 2016

DOI: 10.1021/acs.jpcc.5b11465
J. Phys. Chem. C 2016, 120, 4759−4765

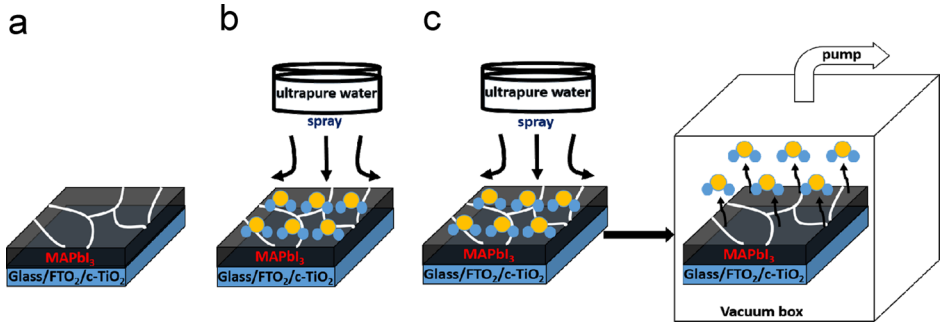

Figure 1. Schematic illustration of treatment on the fully crystallization perovskite film: (a) without any post-treatment (control sample), (b) with vapor spray treatment (sprayed sample), and (c) with vapor spray treatment then vacuum treatment to let the water molecules evaporate from the perovskite film (sprayed/dried sample).

sample that experienced a water vapor spray for 20 s is noted as "sprayed sample" (Figure 1b). The sample that experienced a spraying process and a subsequent drying process by vacuum pumping (let water escape) is noted as "sprayed/dried sample" (Figure 1c). The vapor spraying time is optimized to be 20 s, as shown in Figure S1, Supporting Information. The solar cell devices apply the architecture of FTO/compact-TiO_2/$MAPbI_3$/spiro-MeOTAD/Au configuration. In $I-V$ characteristics, the sprayed sample shows bigger open-circuit voltage (V_{oc}) and short-circuit current (J_{sc}) compared to the control one (Figure 2a), with an improvement in power conversion efficiency (PCE) from 12.6% to 14.7%. Then steady-state output measurements are carried out at the maximum output point (V = 0.7 V) in a nitrogen-filled glovebox under AM 1.5G conditions (100 mW cm^{-2}) (Figure 2b). The control sample shows 10.2% steady-state efficiency, while the efficiency of sprayed sample increases to 12%. To determine whether this enhancing effect can persist after water molecules evaporate from the perovskite crystals, the sprayed/dried sample is also tested. Here vacuum pumping is used in order to accelerate the evaporation process and avoid the unpredictable side effects induced by heat treatment.[20] The results show that the performance of sprayed/dried sample is similar to the control sample and inferior to the sprayed sample in both $I-V$ scan and steady-state measurement (Figure 2a and 2b), which means that the healing effect of water molecules to perovskite film disappears if water evaporates away. On the basis of these results, we can say that vapor spray treatment can improve the performance of perovskite solar cell reversibly.

We speculate some of the possible influences of water molecules on perovskite films here: changing the phase of perovskite crystals and the film morphology or removing excess MAI due to the greater mobility in the presence of water molecules.[18] First, in the work by Yang et al.,[21] it was mentioned that a hydrated compound of $MA_4PbI_6{\cdot}2H_2O$ was found when a small amount of water (60 μL) was added into perovskite powder (200 mg) while there was a small amount residual $CH_3NH_3PbI_3$ without any PbI_2 present. However, scanning electron microscopy (SEM) images (Figure 3a and 3b) and X-ray diffraction (XRD) spectra (Figure 3d) show no difference in morphology and composition between sprayed sample (optimum condition, 20 s) and control sample. Further elongating the spraying time to 30 and 60 s will degenerate the film into lead iodide (PbI_2), as shown in Figure 3c and 3d. This result is different from the work by Yang et al.,[21] which may be attributed to different preparation method. Thus, we confirm that water molecules do not influence the phase and morphology of perovskite films within the optimum spraying time.

In order to investigate how water molecules impact the quality of perovskite films and the photovoltaic performance of solar cell devices, we carry out various measurements on the samples. The Urbach energy (Eu) was used to characterize the defect states within the band gap of perovskite film. Urbach energy can be expressed by $A(E) \approx e^{E/Eu}$, where A is the absorbance and E is the excitation energy.[22,23] The linear fit to the Urbach tail gives a Urbach energy of ~35 meV for control sample, ~26 meV for sample sprayed for 20 s, and ~38 meV for sample sprayed for 60 s (Figure 2c). These results indicate a significant influence of water molecules on the quality of perovskite crystals: 20 s spraying gives a better film quality than control and 60 s sprayed samples.

PL mapping was conducted to further investigate the role of water molecules on perovskite film. Figure 4a and 4b shows the PL mapping in a fixed region of about 9 × 9 μm^2 on a perovskite film before and after vapor sprayed for 20 s. The enhanced PL intensity in almost the entire region indicates that water molecules improve the quality of overall perovskite film. Figure 4c depicts the optical image of the tested region. The steady-state PL measurement (Figure 4d) shows a tremendous increase in PL intensity for the sample sprayed for 20 s and an obvious blue shift of about 12.5 nm compared to control sample. These results imply a suppressing effect of the nonradiative recombination in perovskite crystals induced by water molecules.

In order to confirm our hypothesis, we performed the time-resolved photoluminescence (TRPL) test using the time-correlated single-photon counting method. The charge carrier lifetime in the perovskite is strongly dependent on the polycrystalline nature of the film and the defect density or electronic trap density within the films.[22] The perovskite film showed a longer minority carrier lifetime after vapor spray (Figure 5a). However, its lifetime decreased to the initial value after vacuum drying treatment, which can extract the water molecules away from the films. This was more evidence for the reversible deactivation effect of the water molecules to the deep-level defects in perovskite films. Considering the volatility of water molecules under regular ambient, we carried out the TRPL tests for the sample before and after vapor spray treatment with time to figure out the dynamic influence of the water molecules (Figure 5b). For the sample kept for 10 min after vapor spraying, the charge carrier lifetime increased from 150 to 240 ns compared to the result before vapor spray. Furthermore, the lifetime decreased to 176 ns when the sample

DOI: 10.1021/acs.jpcc.5b11465
J. Phys. Chem. C 2016, 120, 4759−4765

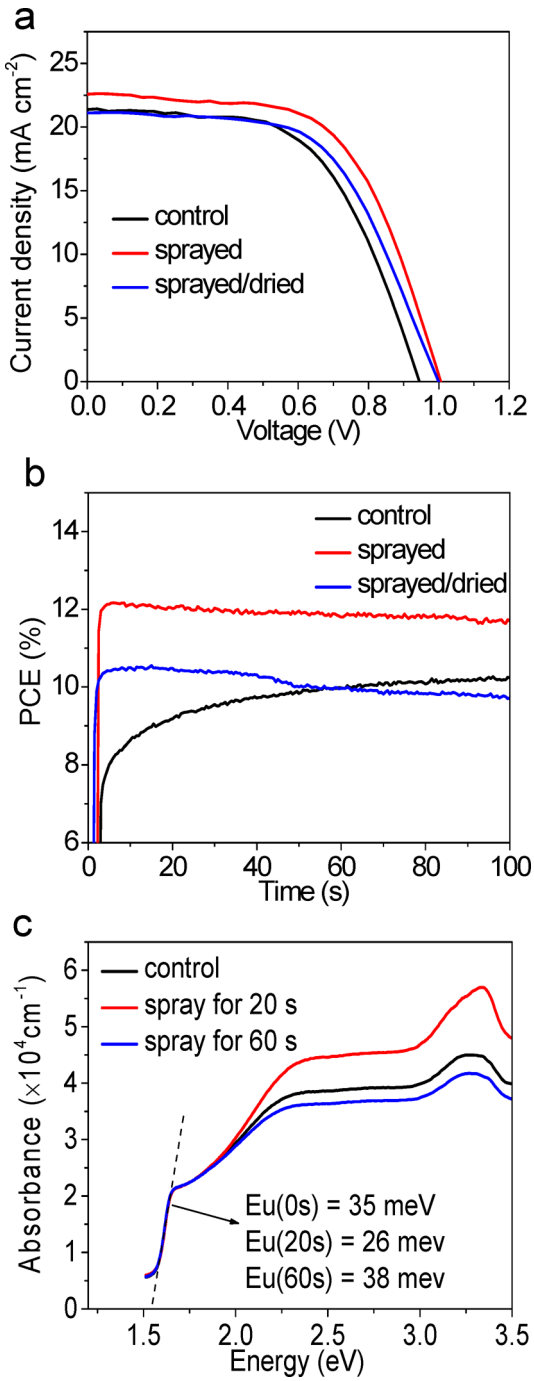

Figure 2. (a) Reverse current−voltage scan for perovskite solar cells made with control, sprayed, and sprayed/dried perovskite films. (b) Stabilized power output measurements for perovskite solar cells made with control, sprayed, and sprayed/dried perovskite films. (c) Absorption spectra of control sample and sprayed sample for vapor spray of 20 and 60 s. The linear fit (dotted line) of the Urbach tail is used to obtain the Urbach energy (Eu). Absorbance was normalized at the band edge ≈ 1.7 eV.

was kept for another 10 min. Referring to our hypothesis, the increment of carrier lifetime of the sample kept for 10 min after spraying is due to the healing effect of water molecules which suppress the nonradiative recombination process. However, with time elongated, MAI would escape from the perovskite crystals with water molecules during evaporation. This escaping behavior will induce some vacancies of MAI on the surface of perovskite film, and these defects can accelerate the nonradiative recombination process, which resulted in a decrease of carrier lifetime for the sample kept for a longer time.

In order to demonstrate that MAI vacancies are detrimental to the charge carrier lifetime, we tested the TRPL of sample before and after heat treatment at 250 °C for 30 s, which will create plenty of MAI vacancies. The charge carrier lifetime decreased from 92 to 48 ns (Figure 5c) after heat treatment and recovered to 90 ns when the heated sample is vapor sprayed for 20 s. The results well support our hypothesis above. Due to the presence of plenty of MAI vacancies, it is not reasonable to explain this increase in carrier lifetime after spraying by removing excess MAI by water molecules. Furthermore, there is no difference in charge carrier lifetime of the films dipped into MAI solution (4 mg/mL in isoproponal) for 20 s (Figure 5d), which implies that excess MAI will not influence the recombination process. On the basis of the TRPL results, we attribute the mechanism of the reversible healing effect of water molecules to deactivating nonradiative recombination centers rather than removing excess MAI.

In order to directly evidence the deactivation effect we proposed above we use the impedance spectrum (IS) to extract the density of defect states in perovskite film, which is a well-established and widely used technique in dye-sensitized solar cells,[23] organic solar cells,[24] and perovskite solar cells.[25,26] Here, in our experiment, the IS measurements were performed under 10 mW cm^{-2} because the perturbation of the data under 100 mW cm^{-2} were too large to be analyzed, which may be caused by the photoinduced reversible structural transformation in perovskite films.[27] We used an equivalent circuit (Figure S2, Supporting Information) to fit the plots and then extracted related recombination time constants ($\tau_{rec} = R_{rec} \times C_{rec}$). Figure 6 shows the τ_{rec} extracted under different bias voltages (V_{bias}) for the three types of samples. It is shown that τ_{rec} increase about 200% around V_{bias} = 0 V and 150% around V_{oc} after vapor spray (Figure 6a and 6b), indicating that water molecules can effectively suppress the recombination process in devices. Additionally, the sprayed/dried sample has a shorter τ_{rec} compared to the sprayed sample. This decrease of τ_{rec} can be attributed to the defect states induced by evaporation of water molecules.

The density of defect states can be derived by the angular frequency-dependent capacitance using the equation[28,29]

$$N_t(f) = -\frac{(V_{bi} - V_{app})}{qW}\frac{dC}{df}\frac{f}{kT} \quad (1)$$

where V_{bi}, W, and V_{app} stand for the build-in voltage, width of the space charge region, and applied voltage, respectively. Then the X axis should be turned from frequency to energetic distance $E_a = E_t - E_x$ ($E_x = E_c$ or E_v) using thermal admittance spectroscopy (TAS).[30] Finally, we have the energetic defect distribution under different applied bias voltages as the equation

$$N_t(E_a) = -\frac{(V_{bi} - V_{app})}{qW}\frac{dC}{df}\frac{f}{kT} \quad (2)$$

as shown in Figures 7a−c and S3, Supporting Information. In the control sample, there are two defect states: one located at a shallow level (E_a < 0.27 eV) and another located at a deep level (E_a = 0.295 eV) (Figure 7a). However, the two defect states change into one locating around E_a = 0.28 eV in the sprayed sample (Figure 7b). In contrast, the sprayed/dried sample also

DOI: 10.1021/acs.jpcc.5b11465
J. Phys. Chem. C 2016, 120, 4759−4765

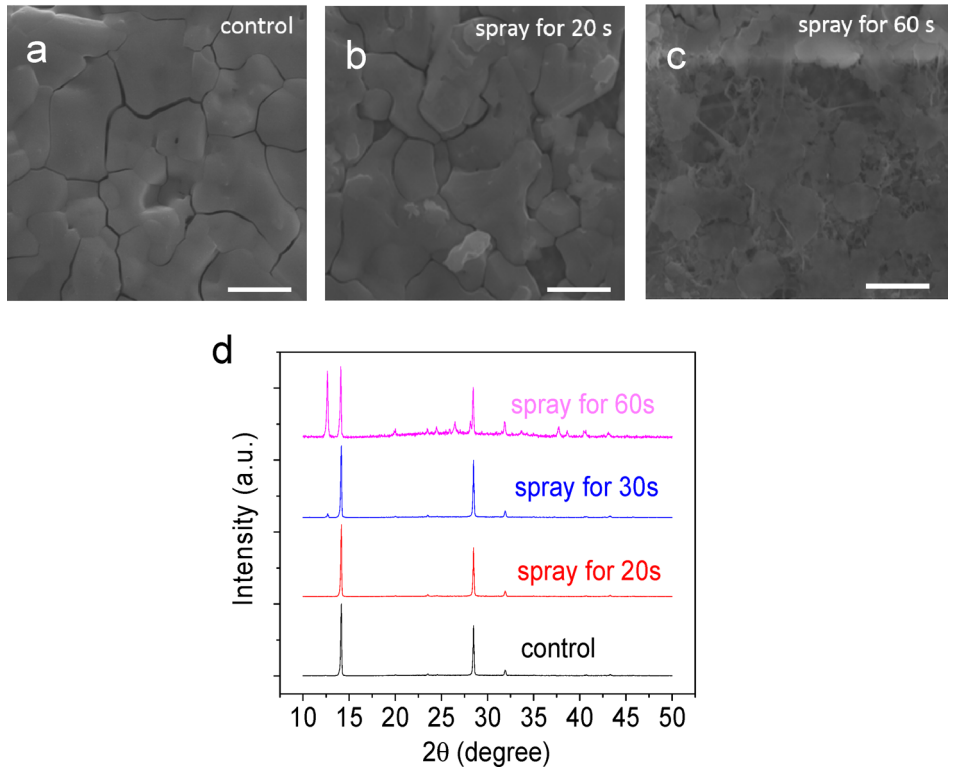

Figure 3. SEM images of (a) control, (b) vapor spray for 20 s, and (c) vapor spray for 60 s perovskite films. Scale bar: 1 μm. (d) XRD spectra for control (black), spray 20 s (red), spray 30 s (blue), and spray 60 s (pink) perovskite films.

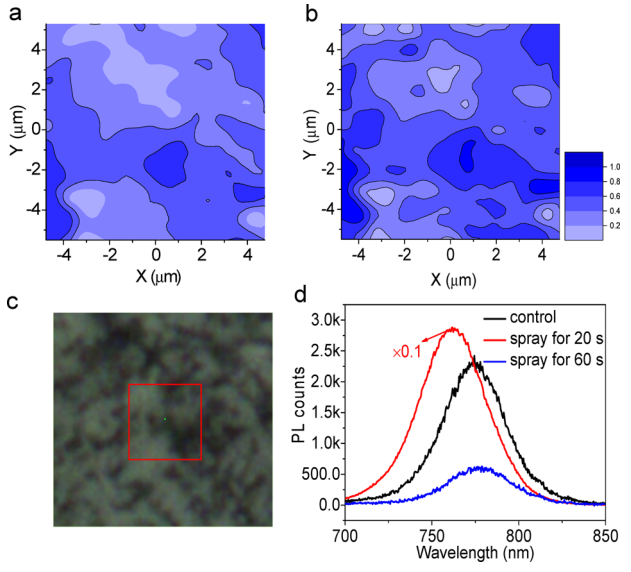

Figure 4. Photoluminescence mapping tests on a 9 × 9 μm^2 region of perovskite film (a) before and (b) after vapor spray for 20 s. (c) Optical microscope image of the perovskite film before vapor spray. Red square represents the 9 × 9 μm^2 PL test region. (d) In situ steady PL measurement on a perovskite film before (black line) and after vapor spray for 20 s (red line) and 60 s (blue line).

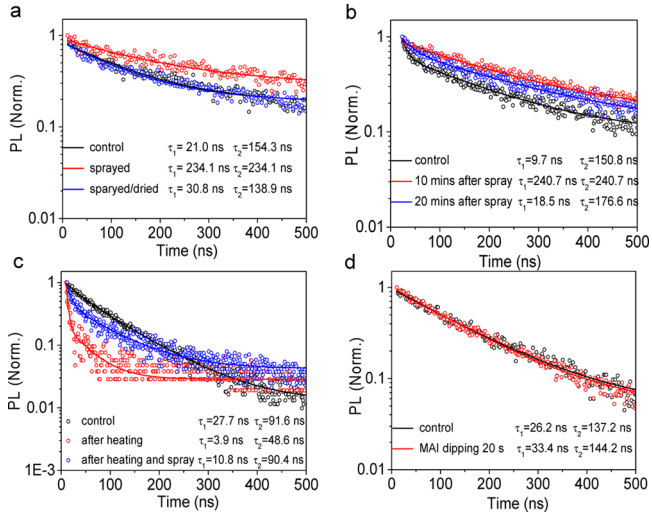

Figure 5. (a) TRPL of control (black line), sprayed (red line), and sprayed/dried (blue line) perovskite films. (b) TRPL of control (black line), 10 min after spray (red line), and 20 min after spray (blue line) perovskite films. (c) TRPL of perovskite films before heat treatment (black line), after heat treatment (red line), and vapor spray after heat treatment (blue line). (d) TRPL of control (black line) and after MAI dipping for 20 s (red line) perovskite films.

has two defect states which overlap with each other to some extent (Figure 7c). The results suggest that water molecules can heal perovskite crystals by changing defect states from deep level to shallow level reversibly.

It is very challenging to directly prove the interaction between water molecules and perovskite crystal by means of H^1 nuclear magnetic resonance (NMR) for the reaction between water molecules and the deuterated DMF or DMSO solvent. In the work by Li et al.,[31] hydrogen bonding between the hydroxyl in phosphonic acid (−PO(OH)$_2$) end groups of the 4-ABPACl species and the iodide ion had been identified by NMR data. It is believed that the hydroxyl in the water molecule and iodine ion in perovskite crystal can also bond in the same way. Because of the strong polarity in the water molecule, this interaction will be nontrivial, leading to an extra energy part in

DOI: 10.1021/acs.jpcc.5b11465
J. Phys. Chem. C 2016, 120, 4759−4765

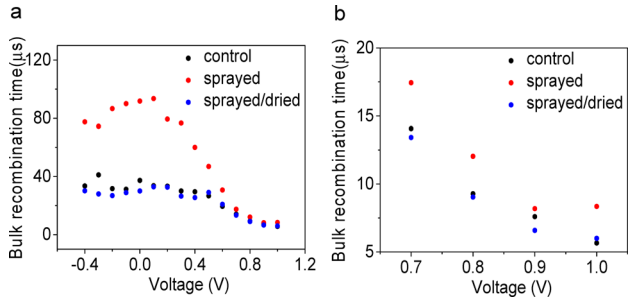

Figure 6. Impedance spectroscopy characterization for charge carrier recombination on devices made of control (black), sprayed (red), and sprayed/dried (blue) perovskite films. (a) Recombination time under different applied bias. (b) Zoom-in impedance spectroscopy from 0.7 to 1.0 V of recombination time.

Sherdinger's equation to describe the electronic surface states. Also, the corresponding energy eigenstate will be shifted to another value. Herein, we found that the energy level of these surface defects decreases after vapor spray, proved by the energetic defect distribution data obtained from IS measurement (Figure 7a–c). If the corresponding energy eigenstate shifts from deep-level states to shallow-level states due to such interaction, we call it defects passivation or deactivation, which had already been demonstrated in previous work.[17,32] This is consistent with the work by Xu et al.,[17] which proved that recombination centers of Pb–I antistite defects can be deactivated upon interacting with PCBM. The deactivation process occurs when water molecules absorb on the perovskite film (Figure 7d to 7e) and the defect states distribution change to the initial state after water molecules evaporate from the film (Figure 7e to 7f). We know that defects like interstitials or antisites associated with Pb and I form electronic trap states inside the band gap and deep defect states (E_{trap} > 250 meV),[33] which strongly capture both free charge carriers. This process induces accelerated recombination and is highly detrimental to device performance. Thus, the deactivation effect can improve the photovoltaic performance of perovskite solar cells by reducing the nonradiative recombination centers.

In summary, we found that water molecules can improve the quality of perovskite films and promote the device performance reversibly. To find the origin of the reversible healing effect, we investigated the influence of water molecules through the change of carrier lifetime, recombination time constant, and density of defect states. On the basis of our research, the hydrogen bonding between the hydroxyl in water and the iodide ion in perovskite is believed to induce the deactivation process, changing the deep defect states to shallow ones and resulting in a reversible healing effect. Due to the reversibility of this healing effect, water molecules may be not an ideal material to heal the perovskite crystal. However, this study opens up opportunities for more stable molecular modification with hydroxyl on perovskite films to improve the device performance.

METHODS

Device Fabrication. All chemicals were purchased from Sigma-Aldrich or J&K Scientific Ltd. unless otherwise stated. The photovoltaic devices were fabricated on FTO-coated glass (Pilkington, Nippon Sheet Glass). First, laser-patterned, FTO-coated glass substrates were cleaned in deionized water, acetone, and ethanol followed by ultraviolet treatment for 10 min. Compact layers were deposited on the substrates by spin coating titanium diisopropoxide bis(acetylacetonate) solution

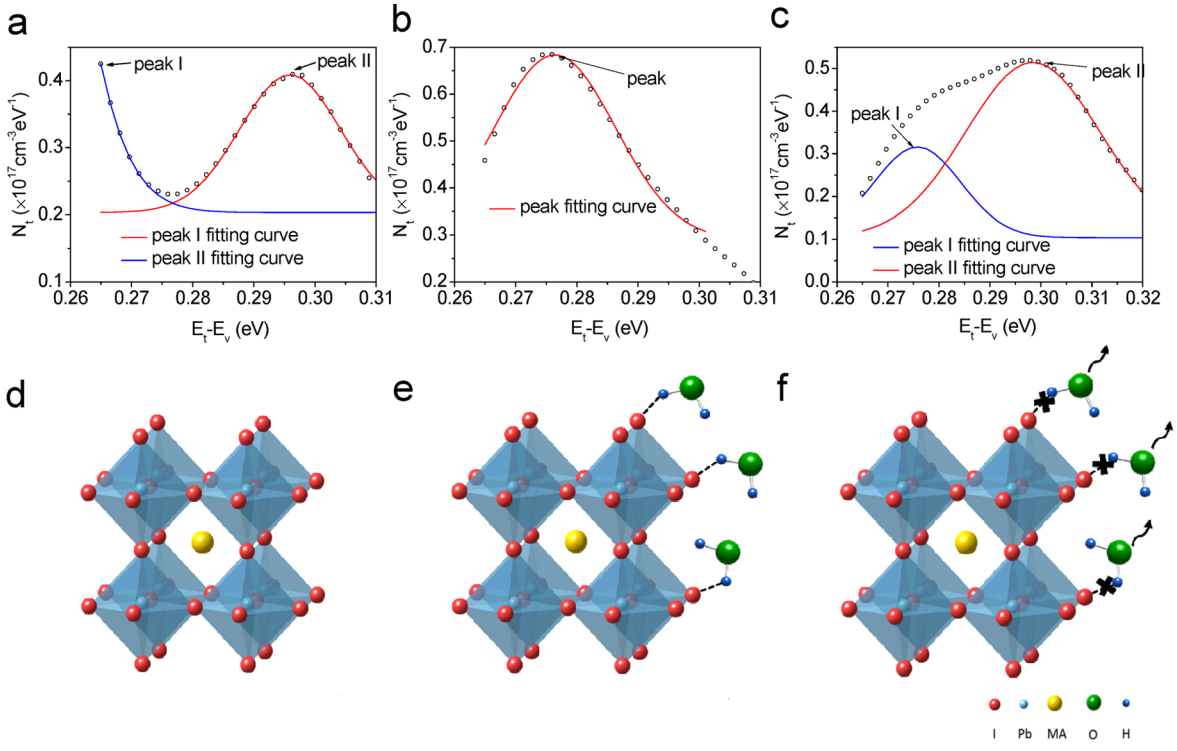

Figure 7. Defect density of states obtained by thermal admittance spectroscopy for devices made of (a) control, (b) sprayed, and (c) sprayed/dried perovskite films under 0.7 V. Schematic illustration of (d) perovskite crystals before vapor spray, (e) interaction between water molecules and perovskite crystals after vapor spray, and (f) disappearance of the interaction after water molecules escape.

DOI: 10.1021/acs.jpcc.5b11465
J. Phys. Chem. C 2016, 120, 4759–4765

(75% in 2-propanol) diluted in ethanol (1:20, volume ratio) two times and annealed at 450 °C for 30 min. After cooling to room temperature, the substrates were transferred to a hot plate at 90 °C before spin coating.

CH_3NH_3I and $PbCl_2$ (Aldrich) (3:1) for 430 and 250 mg/mL solution was stirred in DMF at 60 °C for 12 h. The resulting solution was then coated onto the TiO_2/FTO substrate by spin coating at 500 and 2500 rpm (revolutions per minute) for 10 and 30 s, respectively. Then the substrate was dried on a hot plate at 60 °C for 45 min and sintered at 100 and 105 °C for 50/50 min. After cooing to room temperature, the film went through a 2 h postannealing process at 70 °C.

For the spray treatment, we use a supersonic vapor spray instrument and put the prepared perovskite films at the outlet of this instrument vertically. The supersonic vapor spray instrument was fixed at one-tenth of its maximum power and then sprayed for different times. For the vacuum treatment, the sprayed films were put in a vacuum container immediately after spray treatment and then pumped constantly for 30 min.

The hole transport material (HTM) was spin coated onto the perovskite film at 3000 rpm for 40 s. The spin-coating formulation was prepared by dissolving 72.3 mg of 2,2′,7,7′-tetrakis(*N*,*N*-*p*-dimethoxy-phenylamino)-9,9′-spirobifluorene-(spiro-MeOTAD), purchased from Yingkou OPV Tech New Energy Co. Ltd., 30 mL of 4-*tert*-butylpyridine (tBP), and 20 μL of a stock solution of 520 mg/mL lithium bis-(trifluoromethylsulfonyl) imide (Li-TFSI) in acetonitrile in 1 mL of chlorobenzene. Finally, 90 nm thick gold electrodes were deposited on top of the devices by evaporation at ~10^{-4} mbar. The active area of the electrode was fixed at 9 mm^2.

Device Characterization. The current−voltage (J−V) characteristics were obtained using an Agilent B2900 Series precision source/measure unit, and the cell was illuminated by a solar simulator (Solar IV-150A, Zolix) under AM1.5 irradiation (100 mW cm^{-2}). Light intensity was calibrated with a Newport calibrated KG5-filtered Si reference cell. We use a black mask to define the cell's area, and the masking effect is confirmed by testing the J_{sc} with and without it, which has a 5% J_{sc} difference. The J−V curves are tested from 1.5 to −0.2 V with a scan velocity of 100 mV/s. The masked active area is 9 mm^2. For the steady-state efficiency measurement, the applied voltage is fixed at 0.7 V; then the current value is recorded every 0.1 s. After around 3 s, the current increases slowly when the light turns on. All measurements were conducted in the nitrogen glovebox.

For XRD measurement, X-ray powder diagrams were recorded on an X'PertMPD PRO from PANalytical equipped with a ceramic tube (Cu anode, λ = 1.54060A), a secondary graphite (002) monochromator, and a RTMS X'Celerator detector and operated in BRAGG-BRENTANO geometry. The samples were mounted without further modification, and the automatic divergence slit and beam mask were adjusted to the dimensions of the thin films. A step size of 0.008° was chosen and an acquisition time of up to 7.5 min/deg. A baseline correction was applied to all X-ray powder diagrams to remove the broad diffraction peak arising from the amorphous glass slide.

The surface morphology of the perovskite thin film was characterized by scanning electron microscopy (SEM) (Nano430, FEI). The instrument uses an electron beam accelerated at 15 kV.

For PL mapping, the photoluminescence maps were recorded using a HORIBA/LabRAM HR Evolution. The modulated pump laser beam (455 nm) was focused onto the sample with submicrometer resolution using a confocal microscope objective. To collect a map, the sample position was varied with a piezoelectric stage.

Steady-state photoluminescence (PL) spectra were measured using a He−Cd laser (325 nm in wavelength) and green laser (532 nm in wavelength) guided by a microzone confocal Raman spectroscope (Renishaw inVia microRaman system) as the laser beam with a spot size diameter of 2 μm. The collected duration is ~5 ms. The time-resolved fluorescence spectra were recorded with a high-resolution streak camera system (Hamamatsu C10910). We used an amplified mode-lock Ti:Sapphire femtosecond laser system (Legend, Coherent) and a two-stage optical parametric amplifier (OperA Solo, Coherent) to generate the pump beam with a repetition rate of 1 kHz. All samples were excited by 517 nm at room temperature with ~110 nJ cm^{-2}.

The impedance spectrum was measured using a potentiostat/galvanostat (SP-150, Bio-Logic, France). The frequency can be tuned from 0.1 Hz to 1 MHz with 70 data points, and at each point 200 measurements were averaged to smooth the impedance spectra. All samples were measured under 10 mW cm^{-2} using a 1/10 optical attenuator.

■ ASSOCIATED CONTENT

Supporting Information

The Supporting Information is available free of charge on the ACS Publications website at DOI: 10.1021/acs.jpcc.5b11465.

Current−voltage curves for perovskite solar cells made with perovskite films with different vapor spray time, Nyquist plots of device based on perovskite films without spray treatment under 0 and 0.1 V, defect density of states obtained by thermal admittance spectroscopy for three types of devices (PDF)

■ AUTHOR INFORMATION

Corresponding Author

*E-mail: zhaoqing@pku.edu.cn.

Notes

The authors declare no competing financial interest.

■ ACKNOWLEDGMENTS

This work was supported by National 973 projects (2013CB932602, 2011CB707601, MOST) from the Ministry of Science and Technology, China, and the National Natural Science Foundation of China (NSFC51272007, 61571015, 11234001, 91433102, 11327902). Q.Z. acknowledges the Beijing Nova Program (XX2013003) and the Program for New Century Excellent Talents in University of China.

■ REFERENCES

(1) Kojima, A.; Teshima, K.; Shirai, Y.; Miyasaka, T. Organometal Halide Perovskites as Visible-Light Sensitizers for Photovoltaic Cells. *J. Am. Chem. Soc.* **2009**, *131*, 6050−6052.

(2) Kim, H.-S.; Lee, C.-R.; Im, J.-H.; Lee, K.-B.; Moehl, T.; Marchioro, A.; Moon, S.-J.; Humphry-Baker, R.; Yum, J.-H.; Moser, J. E.; et al. Lead Iodide Perovskite Sensitized All-Solid-State Submicron Thin Film Mesoscopic Solar Cell with Efficiency Exceeding 9%. *Sci. Rep.* **2012**, *2*, 591−597.

(3) Etgar, L.; Gao, P.; Xue, Z. S.; Peng, Q.; Chandiran, A. K.; Liu, B.; Nazeeruddin, M. K.; Gratzel, M. Mesoscopic $CH_3NH_3PbI_3/TiO_2$ Heterojunction Solar Cells. *J. Am. Chem. Soc.* **2012**, *134*, 17396−17399.

DOI: 10.1021/acs.jpcc.5b11465
J. Phys. Chem. C 2016, 120, 4759−4765

(4) Lee, M. M.; Teuscher, J.; Miyasaka, T.; Murakami, T. N.; Snaith, H. J. Efficient Hybrid Solar Cells Based on Meso-Superstructured Organometal Halide Perovskites. *Science* **2012**, *338*, 643−647.
(5) Hodes, G. Perovskite-Based Solar Cells. *Science* **2013**, *342*, 317−318.
(6) Burschka, J.; Pellet, N.; Moon, S.-J.; Humphry-Baker, R.; Gao, P.; Nazeeruddin, M. K.; Grätzel, M. Sequential Deposition as A Route to High-Performance Perovskite-Sensitized Solar Cells. *Nature* **2013**, *499*, 316−320.
(7) Liu, M. Z.; Johnston, M. B.; Snaith, H. J. Efficient Planar Heterojunction Perovskite Solar Cells by Vapour Deposition. *Nature* **2013**, *501*, 395−396.
(8) Heo, J. H.; Im, S. H.; Noh, J. H.; Mandal, T. N.; Lim, C. S.; Chang, J. A.; Lee, Y. H.; Kim, H. J.; Sarkar, A.; Nazeeruddin, M. K.; et al. Efficient Inorganic-Organic Hybrid Heterojunction Solar Cells Containing Perovskite Compound and Polymeric Hole Conductors. *Nat. Photonics* **2013**, *7*, 486−491.
(9) Mei, A. Y.; Li, X.; Liu, L. F.; Ku, Z. L.; Liu, T. F.; Rong, Y. G.; Xu, M.; Hu, M.; Chen, J. Z.; Yang, Y.; et al. A Hole-Conductor-Free, Fully Printable Mesoscopic Perovskite Solar Cell with High Stability. *Science* **2014**, *345*, 295−298.
(10) Zhou, H. P.; Chen, Q.; Li, G.; Luo, S.; Song, T. B.; Duan, H. S.; Hong, Z. R.; You, J. B.; Liu, Y. S.; Yang, Y. Interface Engineering of Highly Efficient Perovskite Solar Cells. *Science* **2014**, *345*, 542−546.
(11) Jeon, N. J.; Noh, J. H.; Kim, Y. C.; Yang, W. S.; Ryu, S.; Il Seol, S. Solvent Engineering for High-Performance Inorganic-Organic Hybrid Perovskite Solar Cells. *Nat. Mater.* **2014**, *13*, 897−903.
(12) Im, J. H.; Jang, I. H.; Pellet, N.; Gratzel, M.; Park, N. G. Growth of $CH_3NH_3PbI_3$ Cuboids with Controlled Size for High-Efficiency Perovskite Solar Cells. *Nat. Nanotechnol.* **2014**, *9*, 927−932.
(13) Gratzel, M. The Light and Shade of Perovskite Solar Cells. *Nat. Mater.* **2014**, *13*, 838−842.
(14) You, J. B.; Yang, Y. M.; Hong, Z. R.; Song, T. B.; Meng, L.; Liu, Y. S.; Jiang, C. Y.; Zhou, H. P.; Chang, W. H.; Li, G.; et al. Moisture Assisted Perovskite Film Growth for High Performance Solar Cells. *Appl. Phys. Lett.* **2014**, *105*, 183902−183908.
(15) Zhang, W.; Saliba, M.; Moore, D. T.; Pathak, S. K.; Horantner, M. T.; Stergiopoulos, T.; Stranks, S. D.; Eperon, G. E.; Alexander-Webber, J. A.; Abate, A.; et al. Ultrasmooth Organic-Inorganic Perovskite Thin-film Formation and Crystallization for Efficient Planar Heterojunction Solar Cells. *Nat. Commun.* **2015**, *6*, 6142−6151.
(16) Shao, Y. H.; Xiao, Z. G.; Bi, C.; Yuan, Y. B.; Huang, J. S. Origin and Elimination of Photocurrent Hysteresis by Fullerene Passivation in $CH_3NH_3PbI_3$ Planar Heterojunction Solar Cells. *Nat. Commun.* **2014**, *5*, 5784−5790.
(17) Xu, J.; Buin, A.; Ip, A. H.; Li, W.; Voznyy, O.; Comin, R.; Yuan, M.; Jeon, S.; Ning, Z.; McDowell, J. J.; et al. Perovskite-Fullerene Hybrid Materials Suppress Hysteresis in Planar Diodes. *Nat. Commun.* **2015**, *6*, 7081−7086.
(18) Eperon, G. E.; Habisreutinger, S. N.; Leijtens, T.; Bruijnaers, B. J.; van Franeker, J. J.; dequilettes, D. W.; Pathak, S.; Sutton, R. J.; Grancini, G.; Ginger, D. S.; et al. The Importance of Moisture in Hybrid Lead Halide Perovskite Thin Film Fabrication. *ACS Nano* **2015**, *9*, 9380−9393.
(19) Gong, X.; Li, M.; Shi, X.-B.; Ma, H.; Wang, Z.-K.; Liao, L.-S. Controllable Perovskite Crystallization by Water Additive for High-Performance Solar Cells. *Adv. Funct. Mater.* **2015**, *25*, 6671−6678.
(20) Poglitsch, A.; Weber, D. Dynamic Disorder in Methylammoniumtrihalogenoplumbates(ii) Observed by Millimter-Wave Specroscopy. *J. Chem. Phys.* **1987**, *87*, 6373−6378.
(21) Yang, J.; Siempelkamp, B. D.; Liu, D.; Kelly, T. L. Investigation of $CH_3NH_3PbI_3$ Degradation Rates and Mechanisms in Controlled Humidity Environments Using in Situ Techniques. *ACS Nano* **2015**, *9*, 1955−1963.
(22) Stranks, S. D.; Snaith, H. J. Metal-Halide Perovskites for Photovoltaic and Light-Emitting Devices. *Nat. Nanotechnol.* **2015**, *10*, 391−402.
(23) Bisquert, J.; Fabregat-Santiago, F.; Mora-Sero, I.; Garcia-Belmonte, G.; Gimenez, S. Electron Lifetime in Dye-Sensitized Solar Cells: Theory and Interpretation of Measurements. *J. Phys. Chem. C* **2009**, *113*, 17278−17290.
(24) Fabregat-Santiago, F.; Garcia-Belmonte, G.; Mora-Sero, I.; Bisquert, J. Characterization of Nanostructured Hybrid and Organic Solar Cells by Impedance Spectroscopy. *Phys. Chem. Chem. Phys.* **2011**, *13*, 9083−9118.
(25) Kim, H.-S.; Mora-Sero, I.; Gonzalez-Pedro, V.; Fabregat-Santiago, F.; Juarez-Perez, E. J.; Park, N.-G.; Bisquert, J. Mechanism of Carrier Accumulation in Perovskite Thin-Absorber Solar Cells. *Nat. Commun.* **2013**, *4*, 2242−2248.
(26) Dualeh, A.; Moehl, T.; Tetreault, N.; Teuscher, J.; Gao, P.; Nazeeruddin, M. K.; Graetzel, M. Impedance Spectroscopic Analysis of Lead Iodide Perovskite-Sensitized Solid-State Solar Cells. *ACS Nano* **2014**, *8*, 4053−4053.
(27) Gottesman, R.; Gouda, L.; Kalanoor, B.; Haltzi, E.; Tirosh, S.; Rosh-Hodesh, E.; Tischler, Y.; Zaban, A.; Quarti, C.; Mosconi, E.; De Angelis, F. Photoinduced Reversible Structural Transformations in Free-Standing $CH_3NH_3PbI_3$ Perovskite Films. *J. Phys. Chem. Lett.* **2015**, *6*, 2332−2338.
(28) Herberholz, R.; Igalson, M.; Schock, H. W. Distinction Between Bulk and Interface States in $CuInSe_2/CdS/ZnO$ by Space Charge Spectroscopy. *J. Appl. Phys.* **1998**, *83*, 318−325.
(29) Walter, T.; Herberholz, R.; Müller, C.; Schock, H. W. Determination of Defect Distributions fromAdmittance Measurements and Application to $Cu(In,Ga)Se_2$ Based Heterojunctions. *J. Appl. Phys.* **1996**, *80*, 4411−4420.
(30) Duan, H.-S.; Zhou, H.; Chen, Q.; Sun, P.; Luo, S.; Song, T.-B.; Bob, B.; Yang, Y. The Identification and Characterization of Defect States in Hybrid Organic-Inorganic Perovskite Photovoltaics. *Phys. Chem. Chem. Phys.* **2015**, *17*, 112−116.
(31) Li, X.; Dar, M. I.; Yi, C.; Luo, J.; Tschumi, M.; Zakeeruddin, S. M.; Nazeeruddin, M. K.; Han, H.; Graetzel, M. Improved Performance and Stability of Perovskite Solar Cells by Crystal Crosslinking with Alkylphosphonic Acid Omega-Ammonium Chlorides. *Nat. Chem.* **2015**, *7*, 703−711.
(32) Noel, N. K.; Abate, A.; Stranks, S. D.; Parrott, E. S.; Burlakov, V. M.; Goriely, A.; Snaith, H. J. Enhanced Photoluminescence and Solar Cell Performance Via Lewis Base Passivation of Organic Inorganic Lead Halide Perovskites. *ACS Nano* **2014**, *8*, 9815−9821.
(33) Buin, A.; Pietsch, P.; Xu, J.; Voznyy, O.; Ip, A. H.; Comin, R.; Sargent, E. H. Materials Processing Routes to Trap-Free Halide Perovskites. *Nano Lett.* **2014**, *14*, 6281−6286.

DOI: 10.1021/acs.jpcc.5b11465
J. Phys. Chem. C 2016, 120, 4759−4765